Thermochimica Acta 491 (2009) 84–91

Contents lists available at ScienceDirect

Thermochimica Acta

journal homepage: www.elsevier.com/locate/tca

Thermal genesis, characterization, and electrical conductivity measurements of terbium oxide catalyst obtained from terbium acetate

S.A. Soliman, B.M. Abu-Zied*

Chemistry Department, Faculty of Science, Assiut University, 71516 Assiut, Egypt

ARTICLE INFO

Article history:
Received 5 January 2009
Received in revised form 4 March 2009
Accepted 9 March 2009
Available online 20 March 2009

Keywords:
Terbium acetate
Terbium oxide
Thermal analysis
Electrical conductivity

ABSTRACT

In this paper, the preparation and characterization of crystalline terbium oxide via thermal decomposition of acetate precursor is reported. The decomposition pathway of the parent salt was followed using TGA, DTA, and *in situ* electrical conductivity in air and nitrogen atmospheres. The obtained results indicated that, thermal decomposition of terbium acetate proceeded with the loss of water molecules, in two steps, below 150 °C followed by decomposition in the temperature range of 300–550 °C, throughout different intermediates, to give Tb_4O_7 as a final product. The calcination products, obtained by heating the parent salt for 3 h in air at various temperatures, were characterized using IR, XRD, SEM, nitrogen adsorption, and electrical conductivity measurements. It was demonstrated that Tb_4O_7 represents the major phase for the samples calcined at 600–900 °C. The role of Tb^{3+}–Tb^{4+} redox couple in enhancing the electrical conductivity of the calcination products was also discussed.

1. Introduction

Terbium (III,IV) oxide is a dark brown color material, has the formula Tb_4O_7, though some texts refer to it as $Tb_2O_{3.5}$ or $TbO_{1.75}$. Tb_4O_7 decomposes to sesquioxide (Tb_2O_3) by losing oxygen at around 600 °C under hydrogen atmosphere [1]. Tb_4O_7 is almost thermally stable to about 1000 °C, however it slightly decomposes (~2%) at high temperatures due to the formation of Tb_2O_3 and $TbO_{1.823}$ [1]. In this context, it is worth mentioning that terbium oxides comprise a series of non-stoichiometric oxides, TbO_x, $x = 1.714$, 1.818, and 1.875 [2,3].

Terbium oxide containing materials have been the object of considerable scientific and technological interest due to their distinctive optical, electronic, and magnetic properties (see for example Refs. [4–10]). With regard to its catalytic activity, it was reported that, for the oxidative dehydrogenation of ethane, doping of $SrCl_2$ with Tb_4O_7 (40 mol%) significantly reduced C_2H_4 deep oxidation and enhanced C_2H_4 selectivity and C_2H_6 conversion [11]. Adding terbium oxide to CeO_2 increases its activity during successive catalytic cycles for soot oxidation [12]. Mixed oxides containing Zr, Ce, Pr and Tb (binary, ternary, and quaternary) exhibit the oxygen storage capacity (OSC) and oxygen transfer capacity (OTC) property under oxidizing and reducing conditions and therefore are important components of three-way catalysts (TWC) [13–17]. In this regard, it was shown that (OSC) of pure CeO_2 is deactivated when the exhaust temperature exceeds 850 °C, due to sintering of the CeO_2 particles and decrease in surface area [17]. Adding terbium oxide to ceria has the following advantages: (i) it stabilizes significantly (in comparison to pure ceria) both specific surface area and small particles sizes during high temperature calcination (up to 1100 °C) [7] and (ii) it increases both oxygen desorption at lower temperatures and the formation of oxygen vacancies, compared with pure ceria [13,17].

The low activity of some catalysts towards NO direct decomposition was related to the formation of adsorbed oxygen accompanying the dissociation of NO which is strongly bonded to the catalyst surface. Thus, poisoning NO dissociation sites and preventing further NO dissociation [18]. Based on the OTC and OSC of terbium oxide, Chuang and Tan [18] have demonstrated that the addition of Tb oxide to Pt/Al_2O_3 allows oxygen from dissociated NO to desorb at temperatures as low as 320 °C, which is significantly lower than that reported for Pt catalysts.

Tb_4O_7 can be obtained by the thermal decomposition of a suitable precursors. Wendlandt [19] reported that, during the decomposition of hydrated terbium oxalate, stable lower hydrates and oxycarbonates were formed as intermediates leading finally to the formation of Tb_4O_7. D'assunção [20] reported the formation of Tb_4O_7 via the thermal decomposition of hydrated terbium basic carbonate. The formation of oxycarbonate phase as intermediate, like other rare earth elements was also reported, during the thermal decomposition of terbium formate [21] and terbium malonate [22]. The formation of Tb_4O_7 was also reported as a final decomposition product of complexes

* Corresponding author. Tel.: +20 122942778; fax: +20 882342708.
E-mail addresses: sa_soliman@yahoo.com (S.A. Soliman), babuzied@aun.edu.eg (B.M. Abu-Zied).

0040-6031/$ – see front matter © 2009 Elsevier B.V. All rights reserved.
doi:10.1016/j.tca.2009.03.006

of 2,5-dichlorobenzoic acid [23] and 2-hydroxybenzoic acid [24].

In the open literature, to the authors best knowledge, no references were found concerning the preparation, characterization, and the application of thermal methods of analysis in the study of terbium oxide catalyst obtained from terbium acetate. Therefore, the present paper reports a physico-chemical studies on terbium oxide obtained via the thermal decomposition of terbium acetate precursor. Thermal events accompanying the thermal decomposition of the starting material were examined by TGA, DTA, and *in situ* electrical conductivity. The solid products formed at 150–900 °C as well as terbium acetate were characterized using XRD, IR, SEM, N_2 adsorption, and electrical conductivity measurements.

2. Experimental

Terbium acetate tetrahydrate, $Tb(CH_3COO)_3{\cdot}4H_2O$, used was 99.9% pure (Aldrich Chemicals). It was calcined at 150–900 °C, in air atmosphere, for 3 h. The calcination temperatures were chosen based on the thermal analysis results (vide infra) of the parent salt, i.e. TbAc. For simplicity, the calcination products will be referred to by abbreviations Tb-*x*, where *x* indicated the calcination temperature.

The simultaneous TGA and DTA curves of the parent salt (TbAc) were recorded with a Shimadzu DT-60 instrument apparatus using a heating rate of 5 °C min^{-1} in air and nitrogen atmospheres till 900 °C. The average masses of the samples were 10 mg. α-Al_2O_3 was used as a reference in the DTA measurements. IR spectra of parent TbAc as well as its calcination products were performed by the KBr disc technique in the wavelength range 4000–500 cm^{-1}, using Shimadzu 470 infrared spectrophotometer.

The electrical conductivity measurements were carried out using a conductivity cell described by Chapman et al. [25]. The temperature was controlled with a WEMA temperature controller. The resistance measurements were carried out using a Keithley instrument 610C solid-state electrometer.

X-ray diffraction patterns were recorded using a Philips diffractometer (type PW 103/00) using Cu Kα radiation. Nitrogen adsorption isotherms (measured at −196 °C) were obtained by using Quantachrome (Nova 3200 series) multi-gas adsorption apparatus. Scanning electron micrographs were obtained using a JEOL scanning microscope, model JSM-5400 LV. The samples were prepared by the gold sputtering technique.

3. Results and discussion

3.1. Thermal analysis and in situ electrical conductivity measurements

Fig. 1a and b, respectively, depicts the TG thermograms obtained upon heating terbium acetate in air and nitrogen atmospheres. Four weight loss (WL) processes could be observed on heating this salt in air till 900 °C. The first two WL steps, which are maximized at 98 and 132 °C (Fig. 1a), are accompanied by 16.45 and 2.05 WL% (Table 1), respectively. Such weight losses are close to that calculated for the

Table 1
Thermogravimetric data and temperature intervals in the thermal decomposition of terbium acetate.

Decomposition stage	Temperature intervals (°C)	Weight loss (%)	
		Air	Nitrogen
I	40–15	16.45	16.55
II	115–60	2.05	1.93
III	200–360 (air), 200–380 (N_2)	32.55	32.35
IV	360–700 (air), 380–700 (N_2)	4.23	4.34

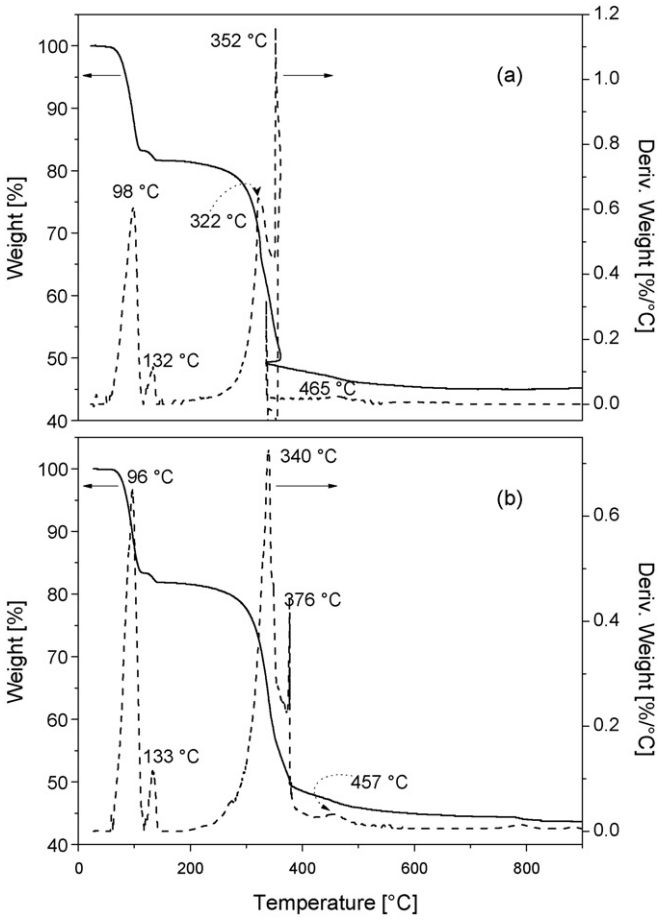

Fig. 1. TGA and DTG curves obtained by heating the parent terbium acetate in air (a) and nitrogen (b) atmospheres.

removal of 3.5 (15.45%) and 0.5 (2.21%) water molecules, respectively, according to:

$$Tb(CH_3COO)_3{\cdot}4H_2O \rightarrow Tb(CH_3COO)_3{\cdot}0.5H_2O + 3.5H_2O \quad (1)$$

$$Tb(CH_3COO)_3{\cdot}0.5H_2O \rightarrow Tb(CH_3COO)_3 + 0.5H_2O \quad (2)$$

Similar trend can be observed on conducting the measurements in nitrogen atmosphere (Fig. 1b). It is of interest to note that this dehydration scheme resembles that reported for samarium acetate tetrahydrate [26]. The third WL step which is located at 200–360 °C in air and at 200–380 °C in nitrogen atmospheres brings a total WL values of 32.55 and 32.35%, respectively. Such WL values matches beautifully with that (32.41%) expected for the formation of terbium dioxy-monocarbonate intermediate. In this regard, many authors [26–32] have shown that the decomposition of many lanthanide anhydrous acetates is accompanied by the formation of metal hydroxy- and oxy-acetate intermediates. Accordingly, step III can be assigned to describe a complex series of overlapping decomposition processes leading eventually to the formation of $Tb_2O_2CO_3$. The formation of terbium carbonate was confirmed throughout the structural analysis of the 400 °C calcined sample (vide infra). In this regard, it is worth mentioning that terbium oxycarbonate represents an intermediate during the thermal decomposition of other terbium oxide precursors, namely formate [21] and malonate [22]. Moreover, the formation of the metal dioxy-monocarbonate intermediates were, also, reported during the thermal decomposition of other rare earth acetates [26–32]. Furthermore, the ability of lanthanides to form oxycarbonates was related to the fact that carbonate ion is a soft base and therefore favours a soft acid, in other

words, a large lanthanide ion [22]. The final WL step, which covers a wide range of temperatures, proceeds with a loss percentage of 4.23% in air and 4.34% nitrogen. Such values are very close to that (4.4%) expected for the decomposition of terbium oxycarbonate yielding terbium oxide (Tb_4O_7). This finding is reinforced by the results of XRD analysis (vide infra) in which Tb_4O_7 the only oxide phase detected for the 600–900 °C calcined samples.

Based on the previous discussion, the decomposition pathway of the anhydrous terbium acetate can be summarized as follows:

$$4Tb(CH_3COO)_3 \rightarrow 2Tb_2O_2CO_3 \rightarrow Tb_4O_7 \quad (3)$$

It should be pointed out here that, the detection of Tb_4O_7 and not Tb_2O_3 as a final decomposition product in both atmospheres is in accordance with the reported literature data in which Tb_4O_7 decomposes to Tb_2O_3 by losing oxygen at around 600 °C only under hydrogen atmosphere [1]. Moreover, this may suggests that the decomposition of the oxycarbonate intermediate is accompanied by the formation of a mixture of CO and CO_2.

Fig. 2 shows the DTA curves recorded for terbium acetate heated to 900 °C in air and nitrogen atmospheres at 5 °C min^{-1} heating rate. This figure manifests the presence of two endothermic effects located at 105 and 137 °C in air and at 100 and 137 °C in nitrogen. In combination with TGA results (Fig. 1) these two peaks can be assigned to the elimination of crystalline water. These endothermic effects are followed by one exothermic effect at 360 °C in air and two exothermic ones at 327 and 375 °C in nitrogen. In combination with our more recent work on thermal decomposition of praseodymium acetate [28] and with the TGA results (Fig. 1), these exothermic effects can be related to the decomposition of the anhydrous acetate leading to the formation of terbium oxycarbonate. In addition, the high exothermicity shown by the peak located at 360 °C (Fig. 2) is reflected by the disturbance observed in the corresponding TG and DTG curves in the 350–400 °C temperature range (Fig. 1a). Taking into account the fact that combustion process is accompanied by a sharp exothermic effect [33], this exothermic effect can be, also, assigned to the combustion of the organic molecules evolved during the thermal treatment. The absence of any thermal effect during the thermal decomposition of $Tb_2O_2CO_3$ could be attributed to the superposition of two opposing processes, namely decomposition of the oxycarbonate (endothermic) and oxidation of Tb^{3+} to Tb^{4+} (exothermic). However, other effects (atmospheric oxygen fixation which is required for Tb^{3+} oxidation and structural changes

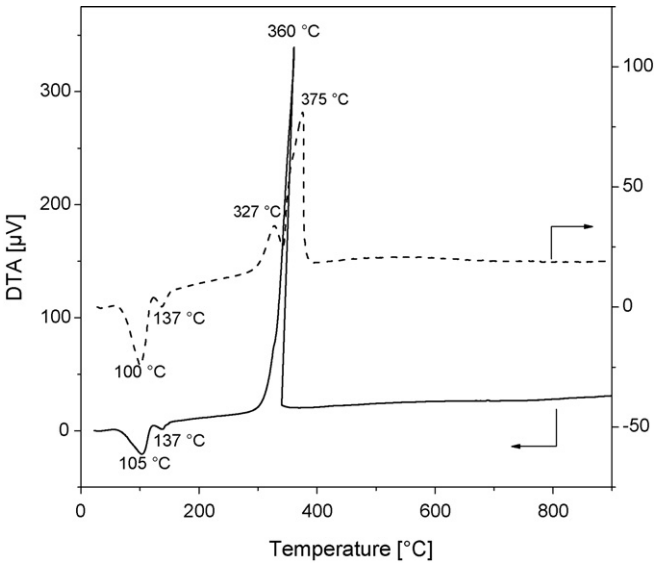

Fig. 2. DTA thermograms obtained by heating the terbium acetate parent in air (solid curve) and nitrogen (dashed curve) atmospheres.

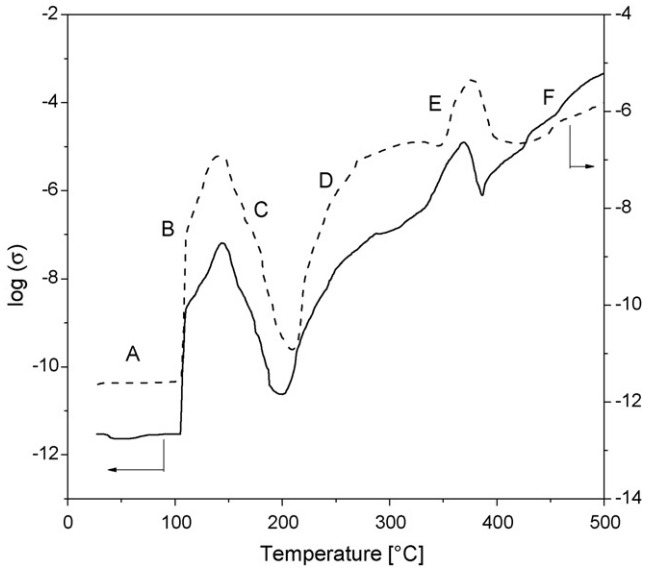

Fig. 3. Plot of log(σ) vs. temperature for terbium acetate during decomposition in air (—) and nitrogen (- - -) atmospheres.

accompanying the oxycarbonate to Tb_4O_7 transformation) cannot be ignored. In this context, the existence of +4 oxidation state of terbium ions have been ascribed to the extra stability associated with the formation of the half-filled $4f^7$ sub-shell [22].

In situ electrical conductivity measurements represent an interesting tool for following up changes accompanying thermal treatment of solids [28,34,35] or during catalytic reactions [36,37]. Temperature dependence of *in situ* electrical conductivity, measured in air and nitrogen atmospheres up to 500 °C (temperature limit of our conductivity cell) is shown in Fig. 3. The obtained plots can be divided into six regions (A–F). In the first region, A (from ambient to 108 °C), nearly constant value of electrical conductivity (σ) is observed. Then a steep increase which is followed by a steady increase can be observed till 140 °C (region B). A continuous decrease in σ can be observed on raising the temperature to 198 °C in air and 211 °C in nitrogen (region C). This decrease is followed by two consecutive conductivity increases till 370 and 377 °C in air and nitrogen, respectively (regions D and E). Finally, a second decrease in σ which is followed by continuous increase in σ till 500 °C can be observed in region (F). In combination with the information inferred from the thermal analysis results (Figs. 1 and 2), the conductivity increase observed in region B can be related to the removal of water molecules leaving back the anhydrous salt. After the completion of the dehydration process a gradual conductivity decrease can be observed (region C). The increase observed in regions D and E can be correlated with the decomposition of the anhydrous acetate to form $Tb_2O_2CO_3$. Thus, it is plausible to attribute the observed conductivity increase to the expected enhancement effect of evolved gases during the decarboxylation process on the mobility of charge carriers. This is in a good agreement with our reported results for the thermal decomposition of praseodymium acetate [28]. Moreover, it goes parallel with the work of Nikumbh et al. [35] who reported an increase in σ during the decarboxylation of copper and zinc malonate, maleate, and succinate complexes. As with what was observed in case of step B, steps D and E are followed by a conductivity decrease as a consequence of ending the decomposition stage. In this context, it is worth mentioning that $Tb_2O_2CO_3$ represents the major phase detected for the sample calcined, for 3 h in air, at 400 °C (vide infra). Finally, the continuous increase in the measured conductivity values observed upon increasing the temperature till 500 °C, event F, is a direct response to the formation of

Tb_4O_7. This matches beautifully with the XRD analysis where Tb_4O_7 represents the major phase detected for the samples calcined at temperatures starting from 500 °C.

3.2. Characterization of the calcination products of terbium acetate

3.2.1. Infrared spectra

IR spectra obtained for the terbium acetate and its calcination products are shown in Fig. 4. Beside the bands at 3800–2700 and 1650–1620 cm^{-1} which are assigned to the ν(OH) and δ(HOH) modes of vibration of crystalline water, the spectrum of the parent salt (Fig. 4a) reveals the presence of absorptions at 1610–500 cm^{-1} which are due to acetate anion [27–31]. These bands are located at 1568, 1455, 1348, (1048 and 1020), 941, 675, and 643 cm^{-1} which are due to the following vibration modes, $\nu_{as}(COO^-)$, $\nu_s(COO^-)$, $\delta_s(CH_3)$, $\rho(CH_3)$, ν(C–C), $\delta(COO^-)$, and $\pi(COO^-)$, respectively. The IR spectrum taken for Tb-150 (Fig. 4b) reveals the persistence of the absorptions due to acetate anion. Meanwhile, a decrease in the intensity of the absorption due to ν(OH) and a disappearance of the δ(HOH) is evident. On raising the pre-treatment temperature to 300 °C, one can easily observe the absorptions due to acetate lattice vibration (Fig. 4c). Further raise in the pre-treatment temperature till 400 °C (Fig. 4d) is accompanied by a disappearance of all absorptions characterizing the acetate anion together with the emergence of new peaks at 1530, 1390, 1340, 1058, 870, and 845 cm^{-1} assignable to oxy-carbonate structure [30,31,33,38]. The obtained spectrum for the Tb-500 sample (curve e) shows absorptions characterizing carbonate phase only. Heating the terbium acetate at temperatures ≥600 °C is accompanied by a disappearance of carbonate absorptions.

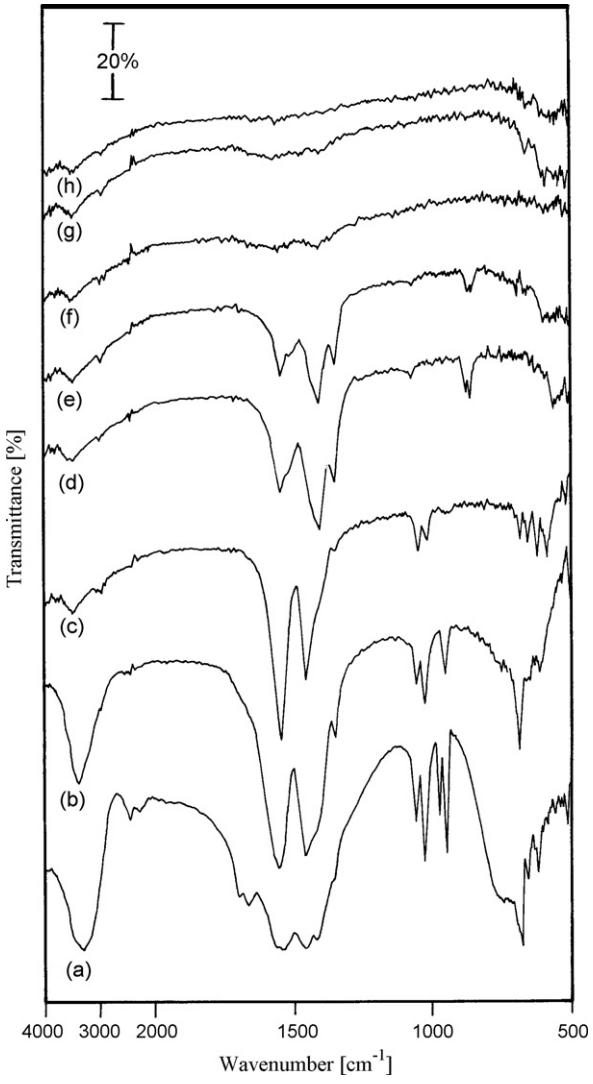

Fig. 4. IR spectra of the terbium acetate parent (a) as well as its calcination products at 150 (b), 300 (c), 400 (d), 500 (e), 600 (f), 700 (g) and 800 °C (h).

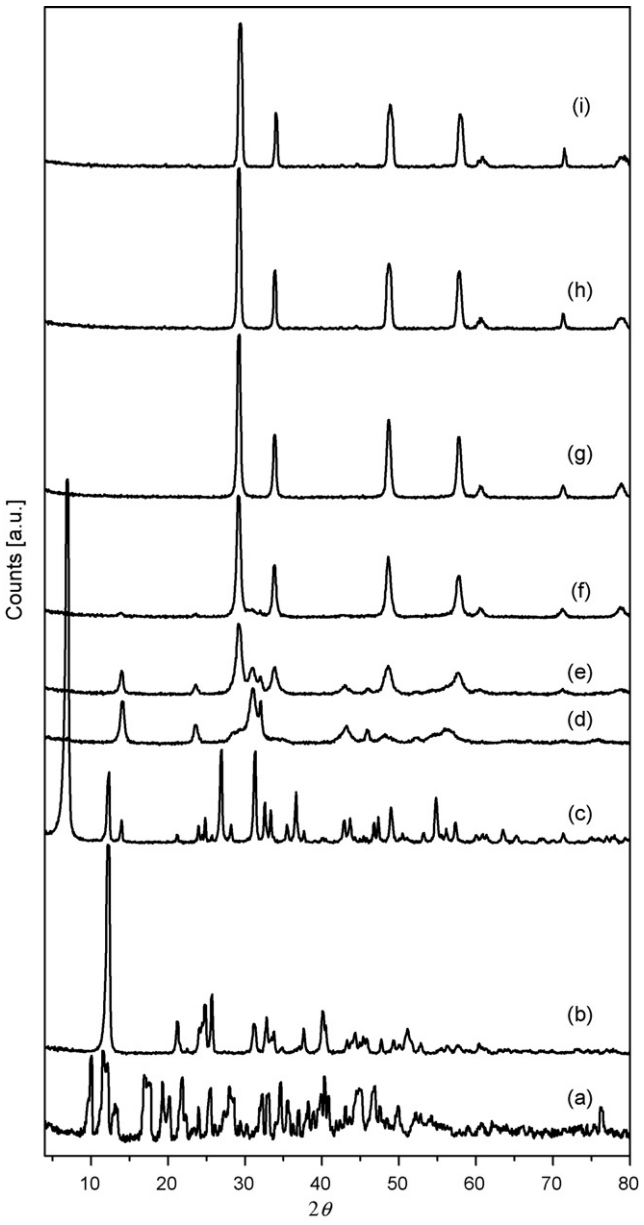

Fig. 5. XRD powder diffractograms obtained for the terbium acetate parent (a) and its calcination products at 150 (b), 300 (c), 400 (d), 500 (e), 600 (f), 700 (g), 800 (h), and 900 °C (i).

3.2.2. X-ray diffraction

X-ray diffraction patterns obtained for terbium acetate and its calcination products formed in air at the 150–900 °C temperature range are shown in Fig. 5. Inspection of this figure reveals that heating the parent salt to 150 °C is accompanied by a noticeable change in the corresponding pattern. At such temperature, and according to our thermal analysis results (Fig. 1), we are dealing

with anhydrous terbium acetate. Thus, one can state safely that, the structure of the hydrated terbium acetate differs from its anhydrous form. Inspection of the XRD pattern of the sample heated at 300 °C (Fig. 5c) reveals the presence of some reflections due the Tb-150 sample together with the emergence of new reflections at 2θ = 6.95, 13.97, 21.18, 26.93, 36.65, 47.32, 48.95, and 54.82. In this respect, IR spectrum of the sample heated at 300 °C (Fig. 4c) showed only absorptions due to acetate and hydroxyl anions. Many authors [26–32] suggested the formation of hydroxy- and oxy-acetates during the thermal decomposition of many lanthanide acetates. Moreover, the XRD pattern (Fig. 5c) is very similar to those reported for the layered Ni–Zn hydroxy-acetates [39–41] with a very intense peak at low diffraction angles (at around 2θ = 6.85) and extremely weak peaks for higher diffraction angles. Checking the available ICDD data bank showed the absence of any card belonging to $Tb(OH)(CH_3COO)_2$ or $TbO(CH_3COO)$. Accordingly, these new reflections could be assigned to the hydroxy-acetate phase. The validity of this suggestion needs further investigation. The diffractogram obtained for the Tb-400 sample demonstrated the disappearance of all reflections exhibited by Tb-300 sample and the appearance of new ones at 2θ = 14.10, 23.63, 31.01, 32.09, 43.19, 45.83, and 56.27. Here, again, inspection of the ICDD data bank revealed the absence of information concerning the $Tb_2O_2CO_3$ phase. However, our IR measurements have demonstrated the presence of absorptions due to carbonate as the only species detected for the Tb-400 sample. Thus, it is plausible to assign these reflections to the presence of terbium oxycarbonate. Increasing the pre-treatment temperature to 500 °C causes a decrease in the reflections attributed to $Tb_2O_2CO_3$ and the emergence of new reflections due to the presence of Tb_4O_7 (ICDD card no. 32-1286) as a major phase. XRD analysis of Tb-600 suggests the co-existence of Tb_4O_7 as a major phase together with trace amount of the oxycarbonate phase. Finally, the XRD patterns of the samples heated at the 700–900 °C temperature range (Fig. 5g–i) are similar among themselves and reveal the presence of crystalline Tb_4O_7 (ICDD card no. 32-1286) as the only phase detected.

3.2.3. Texture analysis and grains morphology

Nitrogen adsorption–desorption isotherms of terbium acetate calcined at 150–800 °C are plotted in Fig. 6. The textural data obtained from the analysis of these isotherms are compiled in Table 2. Inspection of Fig. 6 reveals that the isotherms are approximately belong to type II of Brunauer's classification indicating multilayer adsorption process. Moreover, they are characterized by being irreversible for all samples, and exhibit hysteresis loops close in the low pressure range for all samples. The observed loops are nearly of type H3 [42,43]. The closure point of the hysteresis loops for all the samples is approximately at P/P_0 = 0.1, which indicates either a strong affinity of adsorbate towards the surface or the existence of ultra-micropores [44]. The surface areas were calculated by applying the BET equation whereas S_t values were calculated using the $V_{a\text{-}t}$ plots of de Bore [43]. Following up the variation of S_{BET} values with the calcination temperatures, one can observe a noticeable increase as a result of raising the calcination temperatures from 150 °C to 300–400 °C range, whereas further raise in the heating temperature up to 800 °C is accompanied by a continuous decrease in the measured S_{BET} values. Judging from TGA, IR, and XRD results, the high surface areas of Tb-300 and Tb-400 samples can be attributed to the evolution of gases accompanying the thermal treatment of the parent salt at 300–400 °C temperature range. With further increase in the pre-treatment temperature, we are facing with two opposing effects: (i) evolution of CO_2 which expected to increase the surface areas and (ii) sintering effect which leads to surface area decrease. Thus, it is plausible to suggest that the later effect predominates for the samples heated at temperature higher than 400 °C. On the whole, for all the tested samples,

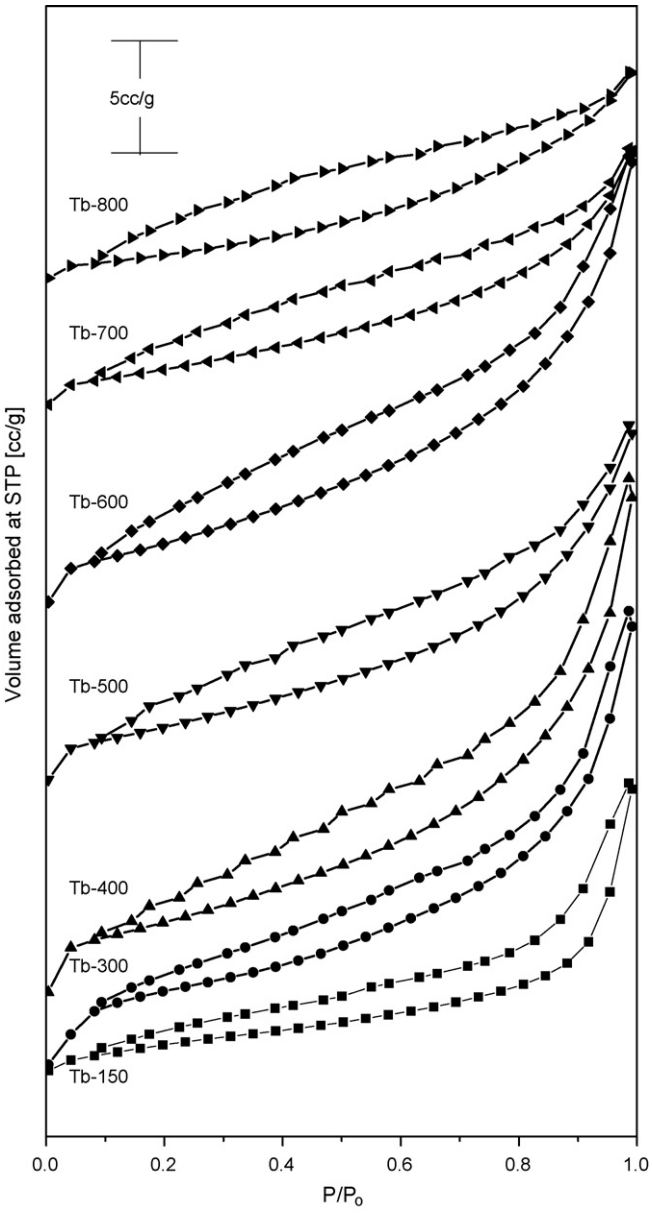

Fig. 6. Nitrogen sorption isotherms for the terbium acetate calcined at various temperatures.

the S_t values obtained from the slope of the linear parts of the $V_{a\text{-}t}$ plots (not shown) agrees satisfactorily with the corresponding S_{BET} values (Table 2).

SEM micrographs of terbium acetate and its calcination products are depicted in Fig. 7. The surface of the original particles (micrograph a) consists of crystals randomly oriented, varying in dimensions, and having sharp edges. Investigation of several crystals of Tb-150 sample (Fig. 7b) demonstrated that the dehydration of the parent salt is accompanied by the formation of more porous network. Moreover, unshaped smaller crystals having some cracks can be observed. The obtained micrographs of Tb-300 and Tb-400 samples (Fig. 7c and d, respectively) show non-parallel plate like particles. In addition, the surface of both samples is covered with randomly distributed pores. Such porous surfaces, which go parallel with the results inferred from the nitrogen adsorption, probably arise as a result of the evolution of gases during the decomposition of terbium acetate. Heating the same solid at 600 °C (Fig. 7e) is accompanied by a dramatic morphological changes. The newly

Table 2
Texture data for the calcination products of terbium acetate.

Calcination temperature (°C)	S_{BET} ($m^2\ g^{-1}$)	S_t ($m^2\ g^{-1}$)	V_p ($\times 10^{-2}\ cm^3\ g^{-1}$)	Average pore diameter (Å)
150	6	9	2.1	134.9
300	15	16	3.2	88.6
400	16	19	3.8	92.9
500	14	14	2.7	79.0
600	14	17	3.3	91.2
700	10	10	2.0	78.9
800	7	9	1.6	90.4

formed solid composed of a coherent-rod like particles extending along the surface. This picture can be considered as supporting evidence for the eventual decomposition of the starting material producing terbium oxide as a final product. Calcining the parent at temperatures as high as 900 °C (Fig. 7f) is accompanied by the formation of large-pitted aggregates having few randomly distributed pores. This picture matches beautifully with the nitrogen adsorption results where Tb-800 sample showed a noticeable decrease in the surface area and the total pore volume.

3.2.4. Electrical conductivity measurements

Electrical conductivity measurements were, also, employed to characterize the 300–900 °C calcination products of terbium acetate. Fig. 8 depicts the dependence of the electrical conductivity

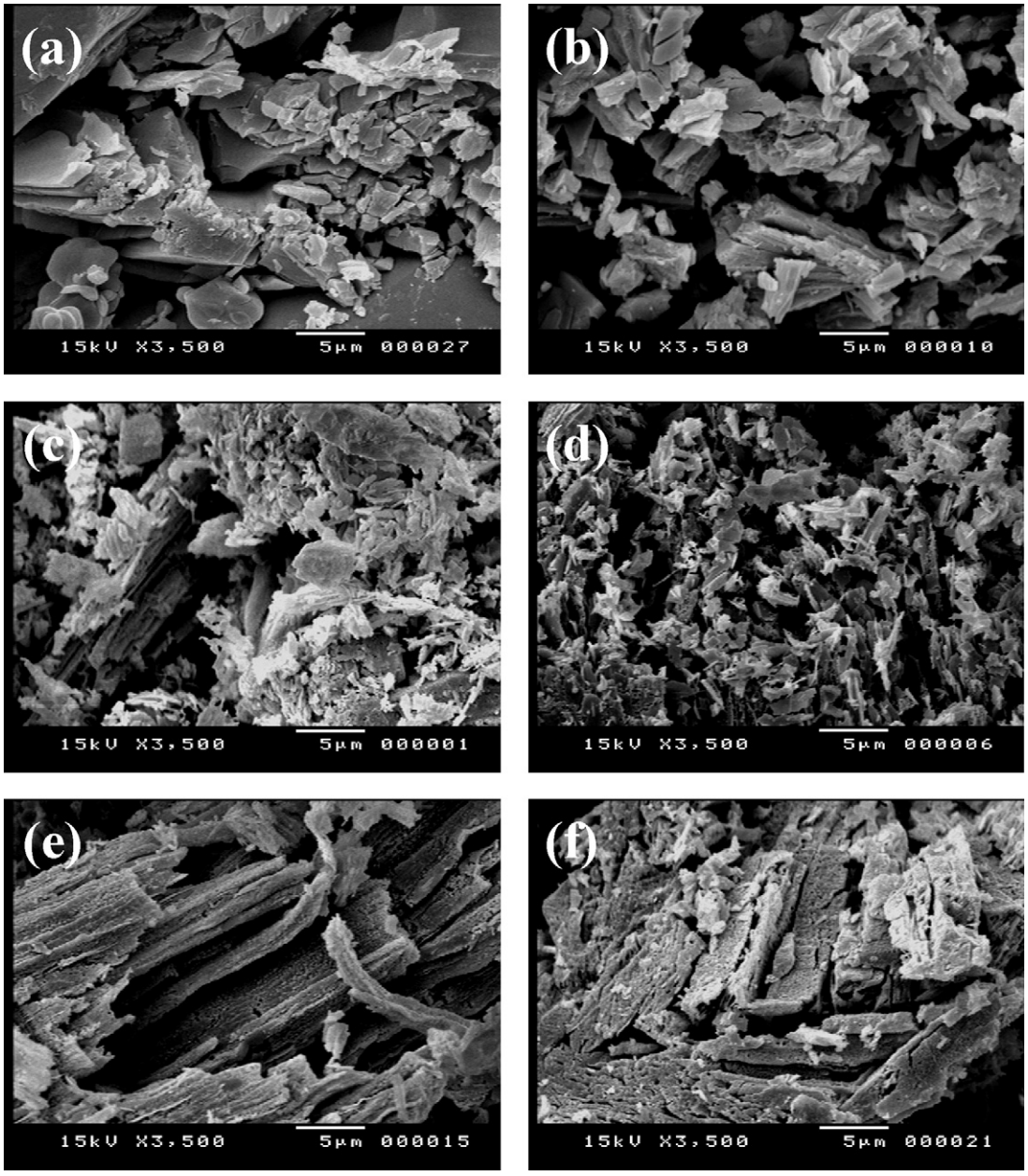

Fig. 7. Scanning electron micrographs obtained for Tb-25 (a), Tb-150 (b), Tb-300 (c), Tb-400 (d), Tb-600 (e), and Tb-900 (f) samples.

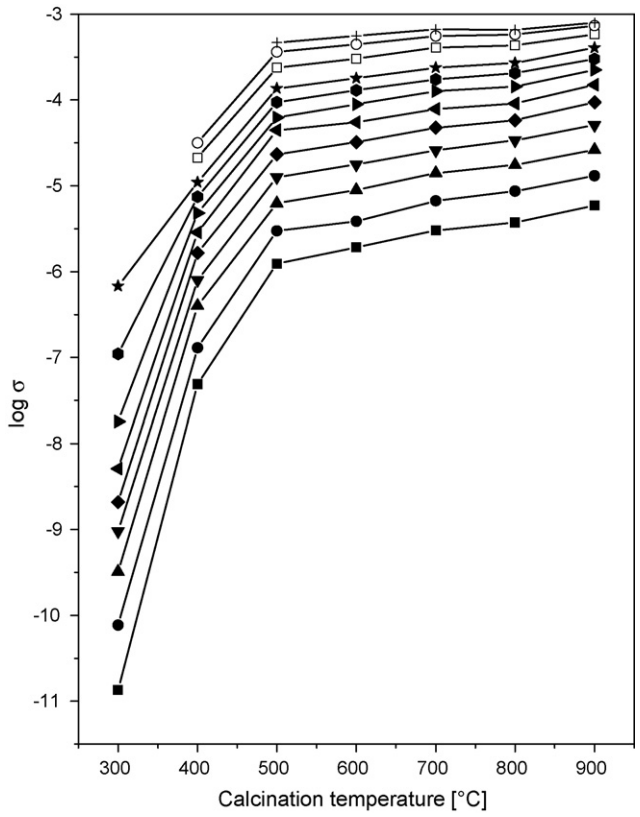

Fig. 8. Dependence of log σ on the calcinations temperature terbium acetate, where the measurements were carried out at 100 (■), 125 (●), 150 (▲), 175 (▼), 200 (♦), 225 (◄), 250 (►), 275 (⬢), 300 (★), 350 (□), 400 (○), and 450 °C (+).

values, log σ, on the calcination temperatures. The measurements were conducted in air atmosphere at the 100–450 °C temperature range. From the inspection of this figure it is evident that the conductivity variation can be divided into two regions: (i) region A for the samples calcined at 300–500 °C and (ii) region B for the samples calcined at 500–900 °C. In region A, increasing the calcination temperatures is accompanied by a sharp conductivity increase. On the other hand, only mild conductivity increase can be obtained on raising the calcinations temperature from 500 till 900 °C (region b). In addition, the trend of conductivity variation with the calcination temperatures is the same all over the whole range of temperature measurements (100–450 °C). A combination between the data presented in Fig. 8 and the conclusions abstracted from TGA, DTA, XRD, and IR analyses suggests that, the trend of conductivity change could be related to the structural changes accompanying the pretreatment of the parent salt in the 300–900 °C range. Consequently, the low values for the 300 and 400 °C calcined samples can be related to the presence of Tb^{3+} containing compounds. The higher conductivity values as well as the continuous mild increase in the conductivity starting from 500 °C can be correlated with the presence of Tb^{3+}–Tb^{4+} couple in the form of Tb_4O_7. In this regard, the idea of the role of the non-stoichiometric nature of terbium oxide in enhancing the electrical conductivity was reported for other systems. Takai et al. [45] showed that substitution of terbium ions in the Pb^{2+} site in $PbWO_4$ is accompanied by conductivity enhancement of one order of magnitude. The reported work over $(Bi_2O_3)_{1-x}(Tb_2O_{3.5})_x$ has indicated that electrons participating in the conduction as the content of terbium increases [46]. Martínez-Arias et al. [7], working on highly homogeneous (Ce, Tb) oxides, stressed the importance of the electron jump between Tb^{4+} and Tb^{3+} in enhancing the electrical conductivity of such system under oxidizing conditions. On similar ground, the high electrical conductivity values characterizing the Cd–Cr–O catalysts was ascribed to the co-existence of high concentration of Cr^{3+}–Cr^{6+} pairs forming the so called mobile-electron Zener phase [34]. Thus, it seems that the presence Tb^{3+}–Tb^{4+} redox couple provides an ideal environment for maximization of the electrical conductivity.

4. Conclusions

The main conclusions gained from this investigation are summarized as follows:

1. The route of thermal decomposition of terbium acetate proceeds firstly with the loss of water molecules, in two steps, below 150 °C. Then the formed anhydrous acetate decomposes in the temperature range of 300–550 °C, throughout different intermediates, to give Tb_4O_7 as a final product. Moreover, the X-ray powder diffraction patterns of the calcination products of TbAc verified the formation of some unreported intermediates during the thermal genesis of Tb_4O_7 from TbAc.
2. The specific surface area and grains morphology depend to a large extent on the calcination temperatures of TbAc. Tb_4O_7 obtained by calcining terbium acetate in air at 600 °C has a surface area of 14 $m^2\ g^{-1}$. Such value drops to 7 $m^2\ g^{-1}$ on calcining the parent salt at 800 °C.
3. Electrical conductivity features shown in this investigation can be correlated to the structural changes accompanying the thermal decomposition of terbium acetate, where the presence of Tb^{3+}–Tb^{4+} redox couple plays a vital role in enhancing the electrical conductivity.

Acknowledgement

The authors would like to thank Prof. Dr. S. Weber (Pittsburg University, USA) for his generous donation of the terbium acetate sample used in this investigation.

References

[1] K.I. Hussain, F. Jasim, Thermochim. Acta 54 (1982) 87–92.
[2] N. Imanaka, T. Masui, Y.W. Kim, J. Solid State Chem. 177 (2004) 3839–3842.
[3] J. Zhang, R.B. Von Dreele, L. Eyring, J. Solid State Chem. 104 (1993) 21–32.
[4] F. Goubard, F. Vidal, R. Bazzi, O. Tillement, C. Chevrot, D. Teyssié, J. Lumin. 126 (2007) 289–296.
[5] R. Bazzi, M.A. Flores-Gonzalez, C. Louis, K. Lebbou, C. Dujardin, A. Brenier, W. Zhang, O. Tillement, E. Bernstein, P. Perriat, J. Lumin. 102/103 (2003) 445–450.
[6] Y. Hinatsu, Y. Doi, J. Alloys Compd. 418 (2006) 155–160.
[7] A. Martínez-Arias, A.B. Hungría, M. Fernández-García, A. Iglesias-Juez, J.C. Conesa, G.C. Mather, G. Munuera, J. Power Sources 151 (2005) 43–51.
[8] F. Ye, T. Mori, D.R. Ou, J. Zou, J. Drennan, Mater. Res. Bull. 43 (2008) 759–764.
[9] G. Wakefield, H.A. Keron, P.J. Dobson, J.L. Hutchison, J. Phys. Chem. Solids 60 (1999) 503–508.
[10] P.A. Tikhonov, M.V. Kalinina, P.V. Rastegaev, I.A. Drozdova, Glass Phys. Chem. 34 (2008) 324–331.
[11] H.X. Dai, C.F. Ng, C.T. Au, J. Catal. 199 (2001) 177–192.
[12] M.A. Małecka, L. Kępiński, W. Miśta, Appl. Catal. B 74 (2007) 290–298.
[13] S. Bernal, G. Blanco, M. Cauqui, M. Corchado, C. Larese, J. Pintado, J. Rodriguez-Izquierdo, Catal. Today 53 (1999) 607–612.
[14] S. Bernal, G. Blanco, M. Cauqui, P. Corchado, J. Pintado, J. Rodriguez-Izquierdo, Chem. Commun. (1997) 1545–1546.
[15] Z. Kang, L. Eyring, J. Solid State Chem. 155 (2000) 129–137.
[16] K. Zhenjin, K. Zhenchuan, J. Rare Earths 24 (2006) 314–319.
[17] F. Guodong, F. Changgen, Z. Zhao, J. Rare Earths 25 (2007) 42–47.
[18] S.S.C. Chuang, C.-D. Tan, J. Phys. Chem. B 101 (1997) 3000–3004.
[19] W.W. Wendlandt, Anal. Chem. 31 (1959) 408–410.
[20] L.M. D'assunção, I. Giolito, M. Ionashiro, Thermochim. Acta 137 (1989) 319–330.
[21] Y. Masuda, Thermochim. Acta 67 (1983) 271–285.
[22] K. Muraishi, H. Yokobayashi, K. Nagase, Thermochim. Acta 182 (1991) 209–217.
[23] W. Brzyska, E. Świta, Thermochim. Acta 231 (1994) 135–142.
[24] P. Kokkonen, L. Palmu, L.H.J. Lajunen, Thermochim. Acta 119 (1987) 285–292.
[25] P.R. Chapman, R.H. Griffith, J.D.F. Marsh, Proc. R. Soc. (London) 224 (1954) 419–426.
[26] G.A.M. Hussein, J. Chem. Soc. Faraday Trans. 90 (1994) 3693–3697.
[27] B.M. Abu-Zied, Bull. Fac. Sci. Assiut Univ. B 31 (2) (2002) 23–38.

[28] B.M. Abu-Zied, S.A. Soliman, Thermochim. Acta 470 (2008) 91–97.
[29] G.A.M. Hussein, H.M. Ismail, Bull. Chem. Soc. Jpn. 67 (1994) 2628–2634.
[30] G.A.M. Hussein, G.A.H. Mekhemer, B.A.A. Balboul, Phys. Chem. Chem. Phys. 2 (2000) 2033–2038.
[31] G.A.M. Hussein, J. Anal. Appl. Pyrol. 29 (1994) 89–102.
[32] G.A.M. Hussein, J. Anal. Appl. Pyrol. 37 (1996) 111–149.
[33] B.M. Abu-Zied, Colloids Surf. A 211 (2002) 27–42.
[34] A.M. El-Awad, B.M. Abu-Zied, J. Mol. Catal. A 176 (2001) 213–226.
[35] A.K. Nikumbh, S.K. Pardeshi, M.N. Raste, Thermochim. Acta 374 (2001) 115–128.
[36] B.M. Abu-Zied, W. Schwieger, A. Unger, Appl. Catal. B 84 (2008) 277–288.
[37] B.M. Abu-Zied, A.M. El-Awad, J. Mol. Catal. A 176 (2001) 227–246.
[38] M. Popa, M. Kakihana, Solid State Ionics 141/142 (2001) 265–272.
[39] M.A. Ballesteros, M.A. Ulibarri, V. Rives, C. Barriga, J. Solid State Chem. 181 (2008) 3086–3094.
[40] R. Rojas, C. Barriga, M.A. Ulibarri, P. Maletb, V. Rives, J. Mater. Chem. 12 (2002) 1071–1078.
[41] R. Rojas, M.Á. Ulibarri, C. Barriga, V. Rives, Micropor. Mesopor. Mater. 112 (2008) 262–272.
[42] P.A. Webb, C. Orr, Analytical Methods in Fine Particles Technology, Micromeritics Instrument Corp., 1997, p. 55.
[43] G. Leofanti, M. Padovan, G. Tozzola, B. Venturelli, Catal. Today 41 (1998) 207–219.
[44] N.A. Eltekova, D. Berek, I. Novák, F. Belliardo, Carbon 38 (2000) 373–377.
[45] S. Takai, K. Sugiura, T. Esaka, Mater. Res. Bull. 34 (1999) 193–202.
[46] T. Esaka, H. Iwahara, J. Appl. Electrochem. 15 (1985) 447–451.